*Archives of Hydro-Engineering and Environmental Mechanics*
Vol. 55 (2008), No. 1–2, pp. 29–43


# A Fractal Approach for Characterizing Microroughness in Gravel Streams

**A. G. Tsakiris**[1], **A. N. Thanos Papanicolaou**

University of Iowa, Department of Civil and Environmental Engineering, IIHR-Hydroscience and Engineering, Iowa City, IA 52242-1585, USA, e-mails: apapanic@engineering.uiowa.edu

(Received May 04, 2008; revised August 29, 2008)

## Abstract

Discrete cluster microforms, or simply clusters, in gravel streams result from organization of particles found in the surface layer of the gravel bed into disconnected patches. Clusters are the outcome of feedback interaction between flow, sediment and stream planform geometry. The complexity of this interaction results in several different cluster shapes, i.e. line, rhomboid and triangular. The objective of this research is to provide a quantitative characterization of cluster shape. To achieve this, we employed a novel method based on fractal theory and used for the shape description of clusters. Our novel method utilized the cell-counting method for the estimation of the areal fractal dimension, $D_A$ for two major datasets, namely fabricated clusters with well-defined shapes, and clusters developed in the laboratory. The principal finding of this research is that the proposed method successfully characterized cluster shape in quantitative terms. Specifically, it was shown that the new approach could identify clusters of different shapes 84% of the time, under different arrangements. This finding is of great importance for bed pattern recognition studies of stream reaches with superimposed roughness elements such as clusters. The findings of the current work could also assist numerical modellers in the development of more representative models of flows over roughness features such as clusters and in the interpretation of results from such models.

**Key words:** cluster, microforms, shape, fractal, cell-counting

## List of symbols

$A_c$ – cluster area,
$b_A$ – ordinate intercept term,
$D$ – fractal dimension,
$D_A$ – areal fractal dimension,
$D_{AL}$ – area-perimeter fractal dimension,
$D_L$ – outline fractal dimension,
$D_{TOP}$ – topological dimension,
$E.R.$ – cluster elongation ratio,

[1] Principal author.

$L_{\max}$ – length of the greater side of a cluster bounding rectangle,
$L_{\min}$ – length of the smaller side of a cluster bounding rectangle,
$L_{obj}$ – characteristic cluster length,
$M_{\max}$ – length of the major axis of the cluster best fitting ellipse,
$M_{\min}$ – length of the minor axis of the cluster best fitting ellipse,
$N(\mu)$ – number of cells of size $\mu$ required to cover the cluster,
$P_c$ – cluster perimeter,
$\mu$ – cell size.

## 1. Introduction

Discrete cluster microforms, or simply clusters, are one type of small-scale roughness feature typically observed in high-gradient gravel streams with limited sediment supply. Clusters have traditionally (Teisseyre 1977, Brayshaw 1984, Strom and Papanicolaou 2007) been differentiated from other small-scale bedforms, such as transverse ribs and clast dams (Bluck 1987), and macroforms, e.g. step-pool sequences (Whittaker and Jaeggi 1982) based on two common characteristics of clusters. These two characteristics are, namely: (1) the size of clusters is of similar order of magnitude with the bed material, i.e. the grain scale and (2) the patches of grouped individual particles are situated atop the gravel bed. Therefore, the term "cluster" is employed to describe these unique microroughness features that arise from the organization of particles found in the stream bed surface layer into disconnected patches (Laronne and Carson 1976, Brayshaw 1984, Reid et al 1992, Papanicolaou et al 2003).

Once developed, clusters have significant effects on bedload transport patterns within a gravel stream reach, which can be distinguished into three phases (Strom et al 2004). First, there is a sink phase coinciding with cluster formation, where clusters absorb incoming sediment from upstream. Second comes a neutral phase, where cluster effects on bedload are minimal. Third, there is a source phase, when clusters begin to disintegrate and thus release sediment. In all three phases clusters contribute to the pulsating nature of the bedload by increasing the amplitude of the fluctuations in the bedload rates. In addition, clusters have a well-documented influence on the near bed turbulence characteristics, which is related to cluster spacing (Buffin-Bélanger and Roy 1998, Papanicolaou et al 2001, Lacey and Roy 2007). It has been suggested that cluster spacing is determined such that clusters induce the maximum resistance to the flow (Hassan and Reid 1990).

Clusters are considered to be the outcome of feedback interaction between the near bed turbulence structure, the available entrainable sediment and stream planform geometry such as sinuosity (Papanicolaou 1999, Strom and Papanicolaou 2007). The stochastic nature of this feedback interaction leads to different cluster shapes. In the field, cluster shapes such as pebble clusters, in-line and ring clusters (Brayshaw 1984, de Jong 1995, Kozlowski and Ergenzinger 1999, Wittenberg

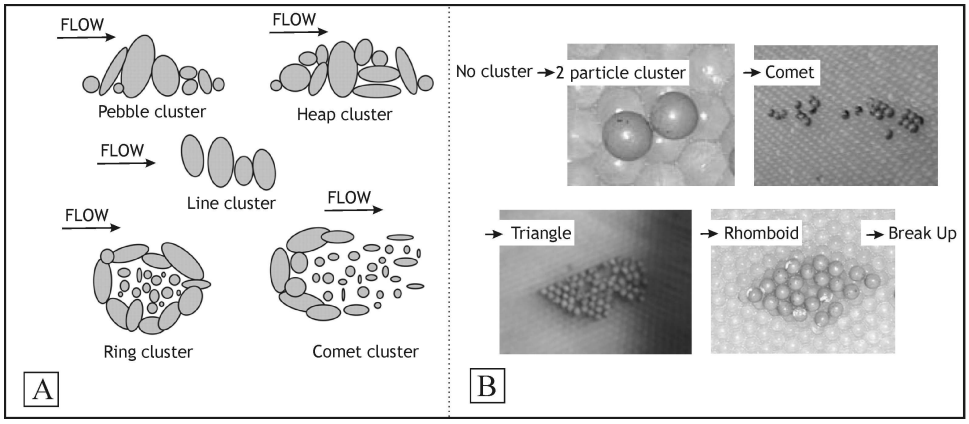


**Fig. 1.** Characteristic shapes of clusters (A) in the field (Strom and Papanicolaou 2007) and (B) in the laboratory (Papanicolaou et al 2003)

2002, Strom and Papanicolaou 2007) have been documented (Fig. 1A). Several cluster shapes (e.g. in-line, rhomboid and pebble clusters) (Fig. 1B) have also been identified in laboratory investigations (Papanicolaou et al 2003, Papanicolaou and Kramer 2005). Furthermore, in the laboratory study of Papanicolaou et al (2003), where the effects of sediment gradation were eliminated via the use of unisize sediment, cluster shape was observed to change with increasing bed shear stress under conditions of limited sediment availability (Fig. 1B). This indicates that cluster shape reflects the prevailing flow conditions. Cluster shape is also dependant on the available entrainable sediment. In natural streams, in-line clusters are formed when sediment of similar size nest together (Strom and Papanicolaou 2007) (Fig. 1A). Formation of cluster shapes, such as the pebble cluster, requires availability of anchor particles and poorly sorted entrainable sediment (Brayshaw 1984, Reid et al 1992, Strom and Papanicolaou 2007). Therefore, characterization of cluster shape could, in turn, provide insight to the underlying flow conditions and to the sediment transport patterns in gravel streams. However, what is lacking is a method that can characterize cluster shape in quantitative terms and relate it with the characteristic cluster shapes of the cluster evolutionary cycle.

Shape description of natural objects in quantitative terms has been achieved with fractal geometry. Fractal geometry (Mandelbrot 1977) was introduced for the study of irregular, non-Euclidean objects or fractals. The irregularity of a fractal is quantified via the fractal dimension, $D$, a positive non-integer number, which strictly exceeds the topological dimension, $D_{TOP}$ of the fractal. $D_{TOP}$ always assumes integer values and is equal to zero, one and two for objects represented as points, lines and surfaces, respectively. For example, the fractal dimension, $D$, of an irregular coastline is in the range $1 < D < 2$, whereas $D_{TOP} = 1$. $D$ attains values closer to two as the irregularity of the line increases.

Most of the previous studies employing fractal shape descriptors (Orford and Whalley 1983, Longley and Batty 1989, Andrle 1996) have focused on the fractal dimension of the outline, $D_L$, of the examined objects. Some studies (Woronow 1981, Lovejoy 1982) have utilized $D_{AL}$, which is a fractal dimension different from $D_L$, to describe the shape of an object. $D_{AL}$ essentially expresses the scaling relationship between the perimeter and the area of the same object observed at different levels of detail (resolutions). A recent study (Cheng 1995) considered the areal fractal dimension, $D_A$, which corresponds to the areal projection (both the outline and the included area) of the object. $D_A$ combines both $D_L$ and $D_{AL}$ of an object (Cheng 1995) and may provide a unique quantitative characterization of the object shape. However, the potential of $D_A$ to characterize the shape of an object was obscured by the complexity of the method for the $D_A$ estimation (Cheng 1995), which required the prior estimation of both $D_L$ and $D_{AL}$.

The goal of this research is to address the shortcomings of the Cheng (1995) method. Specifically, the two objectives of the present study are: (1) to introduce a practical method for the estimation of $D_A$ and (2) to utilize $D_A$, in order to provide a quantitative criterion suitable for the discrimination of the cluster shapes.

## 2. Methodology

### 2.1. Method and Data Selection

The methodological contribution of this study is that cluster $D_A$ is estimated by applying the cell-counting method (CCM) (Dubuc et al 1989, Klinkenberg 1994, Buczkowski et al 1998) to the areal projection of the clusters. The latter circumvents the prerequisite estimation of $D_{AL}$, which would require multiple area and perimeter estimates of the same cluster at different levels of detail. Therefore, with the method considered herein cluster $D_A$ is estimated in a simple and practical manner. The functionality of the adopted method for the estimation of $D_A$ is further enhanced by taking into account two advantages that the CCM has to offer. These are: (1), the plethora of established and well-documented image analysis software packages (e.g. ImageJ) that include a CCM algorithm, and (2) the simplicity of the CCM. CCM only requires a binary (black and white) image, where the object of interest is isolated (thresholded) from the background.

To meet the two objectives stated earlier, fabricated (synthetic) and laboratory cluster datasets were employed. The analysis of the synthetic clusters with the CCM would establish benchmark values of $D_A$ for each shape. The role of the laboratory dataset is to illustrate the applicability of the CCM on quantitative cluster shape characterization using the benchmark values as a reference.

The synthetic clusters were constructed via a drawing software package with their shape corresponding to the characteristic cluster shapes observed by Papanicolaou et al (2003) (Fig. 1B), i.e. triangle, rhomboid, comet and line shapes. Clusters with triangle, rhomboid and comet shapes are hereafter collectively referred to as

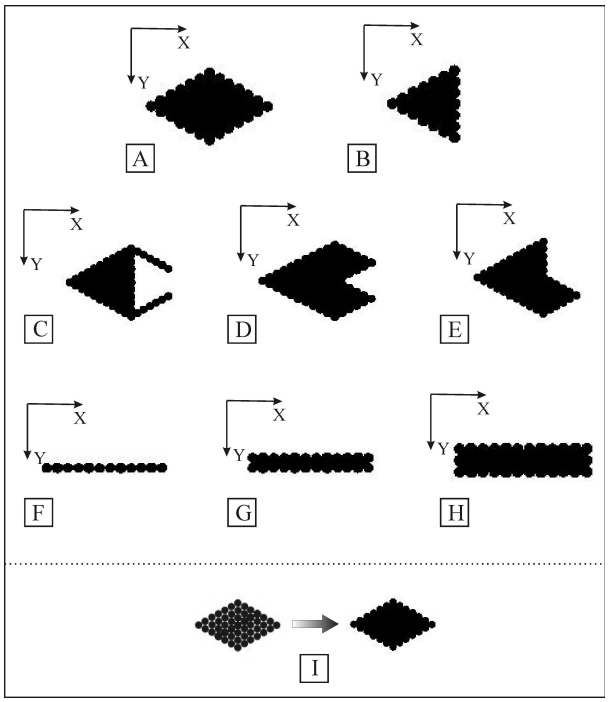


**Fig. 2.** Synthetic cluster shapes and the used coordinate system (A) rhomboid, (B) triangle (C), (D), (E) comet clusters, (F), (G), (H) one, two and three particle wide line clusters, respectively. Cluster "width" is measured along the Y-direction, (I) elimination of the interstices between the circles

2-D or non-linear (in the sense of not being linear) clusters, because the clusters having these shapes are of comparable dimensions along their two directions. Clusters having linear shape are also referred to as 1-D clusters, because one of their dimensions (width) is much smaller than the other (length).

The clusters of the laboratory dataset were formed during the experiments conducted by Strom et al (2004), a continuation of the Papanicolaou et al (2003) study. The laboratory clusters consisted of unisize spherical glass beads 8 mm in diameter and were formed atop a planar bed, consisting of identical spherical glass beads. This laboratory setting eliminated the variability of the clusters in the vertical direction and allowed the study of the horizontal projection of the laboratory clusters

## 2.2. Development of the Fabricated (Synthetic) and Laboratory Cluster Images

Multiple solid circles, 8 mm in diameter, were drawn via the CorelDraw software to fabricate different cluster shapes based on the experiments of Papanicolaou et al (2003). The multiple solid circles were aligned so as to form synthetic clusters having rhomboid shape (Fig. 2A), triangular shape (Fig. 2B), comet shape (Fig. 2C,

2D and 2E) and linear shape. The linear synthetic clusters could have a width (along the Y direction) of one, two or three particles (Fig. 2F, 2G and 2H, respectively). The complete synthetic cluster dataset consisted of five rhomboid clusters, five triangle clusters, nine comet clusters and 16 line clusters, giving a total of 35 clusters. The synthetic clusters of each shape were constructed so as to have similar sizes to the laboratory clusters. The drawing of each synthetic cluster was exported as a black and white image with resolution of 1000 dpi, in which clusters were represented by black pixels and the background with white pixels. The image dimensions were adjusted such that 1 pixel in the cluster images would represent a physical length of 1 mm in every direction of the cluster image. The interstices between the beads were colored black (Fig. 2I) to ensure that the cluster is treated by the software as one single object. The synthetic cluster properties including cluster area, $A_c$, lengths of the sides of the cluster bounding rectangle, $L_{\max}$ and $L_{\min}$ and lengths of the major and minor axes of the best fitting ellipse (denoted as $M_{\max}$ and $M_{\min}$, respectively) were determined via image analysis. An elongation ratio, E.R., for the synthetic linear clusters was calculated as the ratio $L_{\max}/L_{\min}$.

The laboratory clusters considered herein were produced at the final stage of six test runs from the flume experiments of Strom et al (2004), when the bedload rate had stabilized. This way clusters represent a condition of bed equilibrium. Grayscale plan view images depicting the clustered flume bed were used as raw data (Fig. 3A). The images were imported to the public domain software ImageJ (Rasband 1997), where the images were converted to physical length dimensions by specifying the pixel to physical length ratio on the image. The coordinates of the center of each bead in the default coordinate system of the software (Fig. 3A) were manually determined. The clustered beds were plotted as graphs (Fig. 3B). The centers of all the cluster beads were converted to solid circular marks with diameter of 8 pixel units (Fig. 3C). The graphs of the clustered beds were exported as black and white images with a resolution of 1000 dpi and their final dimensions were adjusted so that 1 mm of the laboratory clusters would be represented by 1 pixel (Fig. 3D). In these images, pixels corresponding to particles were of black color, while pixels corresponding to the flume bed were of white color.

"Loose particles" were deposited in the wake regions of existing clusters, due to sheltering effects provided by the existing clusters. Based on the Reid et al (1992) definition, it was reasonable to consider that the "loose particles" are part of the clusters. In the laboratory cluster images, the black pixels representing the "loose particles" were separated from the black pixels representing the existing clusters by white areas. In order to ensure that the "loose particles" were treated as part of the cluster by the software, the white areas were manually colored black (Fig. 3E). Attention was taken not to eliminate the detail of the cluster outline and alter the overall cluster shape. The laboratory cluster geometric properties ($A_c$, $L_{\max}$, $L_{\min}$, $M_{\max}$, $M_{\min}$) were determined via image analysis. The E.R. for the laboratory clusters was calculated as the ratio $M_{\max}/M_{\min}$. The laboratory clusters were each

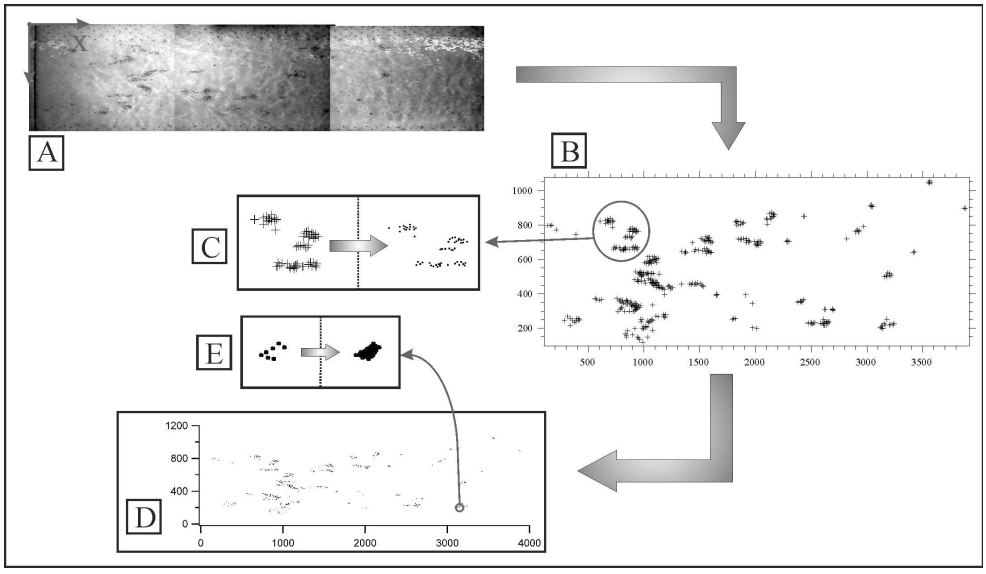


**Fig. 3.** Laboratory cluster methodological steps (A) reconstructed plan view image of a clustered flume bed. Flow is from right to left, (B) graph of the clustered flume bed, (C) conversion and redimensioning of the markers representing the bead centers of two clusters, (D) binary image of the clustered flume bed (E) elimination of the white space corresponding to the cluster wake regions

classified by, means of visual comparison with the characteristic cluster shapes identified by Papanicolaou et al (2003) (Fig. 1B), into one of the four characteristic cluster shape categories. Visual characterization of cluster shape was not feasible for 30 of the 123 laboratory clusters.

### 2.3. Application of the Methodology to the Dataset

The laboratory and the synthetic cluster images were imported to the public domain software FracLac (Karperien 1999–2007) for cell counting analysis. The number of cells, $N(\mu)$, of varying size $\mu$ required to cover the cluster is recorded (Fig. 4). The minimum cell size used was equal to 2 pixel units to account for the cluster boundary crenellation having a characteristic size of 8 pixels. The maximum cell size was set equal to 50% of the object size, $L_{obj}$ (Klinkenberg 1994, Karperien 1999–2007). $L_{obj}$ is defined herein as the length of the greater side of the cluster bounding rectangle and is, thus, equal to $L_{\max}$. A linear progression of cell sizes to span between the minimum and the maximum cell sizes was used (Dubuc et al 1989, Buczkowski et al 1998). The cell counting was repeated four times for each synthetic and laboratory cluster with a different origin point of the cell grid in order to eliminate the dependence of $N(\mu)$ on the grid starting point (Buczkowski et al 1998).

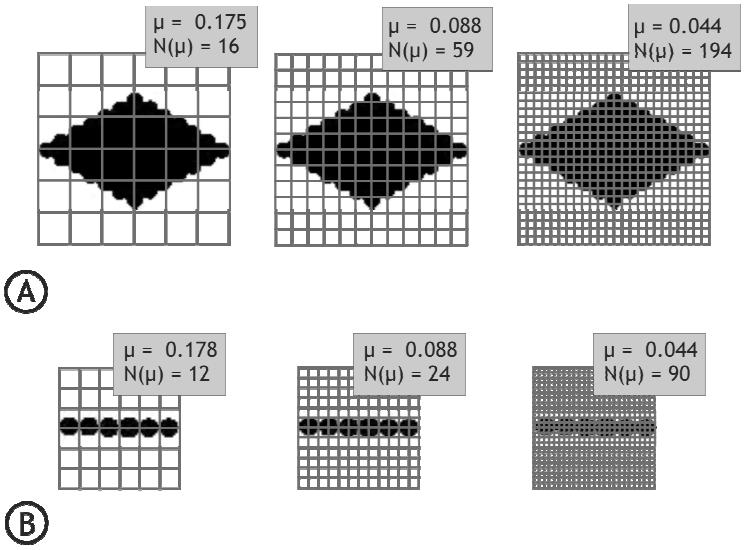


**Fig. 4.** Cell counting method for (A) a rhomboid cluster and (B) a linear cluster, one particle wide. For better visualization, the cell grid is drawn slightly larger than the largest side of the cluster

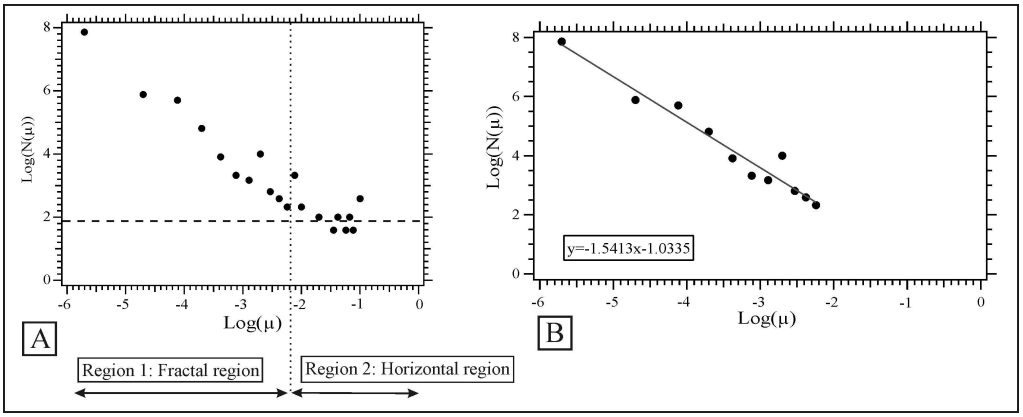


**Fig. 5.** Representative plot of Log(N($\mu$)) vs. Log($\mu$) (A) before the removal of the horizontal band and (B) after the removal

The logarithm of $N(\mu)$ is plotted against the logarithm of $\mu$. A first application of the method revealed that the Log($N(\mu)$) vs. Log($\mu$) datapoints form a horizontal region for larger cell sizes (Fig. 5A). The latter observation suggests that cell sizes within the horizontal region are too large to detect the irregularity of the cluster and thus the cluster is perceived as a smooth Euclidean object (Kaye 1986, Whalley and Orford 1989). Therefore, the Log($N(\mu)$) vs. Log($\mu$) datapoints within the horizontal region should not be considered for the estimation of $D_A$. The horizontal region

is visually identified and removed from the plots (Fig. 5B). $D_A$ is calculated as negative the slope of the best linear fit to the remaining datapoints calculated via least squares regression (Fig. 5B). The ordinate intercept terms, $b_A$, of the regression line are also recorded.

## 3. Results

The distribution of $D_A$ for each characteristic shape of the synthetic clusters, is given in Fig. 6. Only one particle wide clusters (Fig. 2F) are considered for the $D_A$ distributions depicted in Fig. 6, since one particle wide clusters align with the linear cluster shape observed by Papanicolaou et al (2003) (Fig. 1B). Triangle and rhomboid clusters have different ranges of $D_A$ values. Comet clusters have greater variability of $D_A$ values than triangle and rhomboid clusters. Although the higher $D_A$ values of comet clusters overlap with $D_A$ values of rhomboid clusters, the comet and the rhomboid clusters have different median values. Line clusters have $D_A$ values between 1.44 and 1.58, which do not overlap with the $D_A$ values of the other cluster shapes. Therefore, $D_A$ can quantitatively discriminate between the different cluster shapes. In addition, the non-linear clusters (i.e. rhomboid, triangle and comet) have similar $D_A$ values, which are differentiated from the $D_A$ values of the linear clusters. This suggests that similar processes are responsible for the formation of the non-linear clusters as opposed to the linear clusters. However, the high median $D_A$ value of the linear clusters, which approaches the $D_A$ values of the non-linear shapes, indicates that $D_A$ can also capture the succession of the cluster shapes, which is in agreement with the evolutionary cycle of laboratory clusters, as observed by Papanicolaou et al (2003). Linear clusters, which have the lowest values of $D_A$, are the cluster shape formed for the lowest bed shear stress. As shear stress increases, line clusters capture incoming sediment and evolve into comet clusters, which have the next higher values of $D_A$. With further increase in bed shear stress, the triangle clusters, with the highest $D_A$ values, are formed. As the bed shear stress increases further, the triangle clusters turn into rhomboid clusters, which present the most stable shape with slightly lower $D_A$ values prior to the disintegration of clusters (Papanicolaou et al 2003). It is, thus, suggested that $D_A$ can also delineate changes in the prevailing flow conditions, which are reflected with the different cluster shapes.

The $D_A$ values for the complete line cluster dataset plotted against the line cluster E.R. are presented in Fig. 7. Fig. 7 reveals that when E.R. is less than roughly five, the $D_A$ of linear clusters is initially comparable with the $D_A$ of the non-linear clusters, but decreases with increasing line cluster E.R. Above the E.R. threshold value of five, the $D_A$ of linear clusters does not change substantially. This indicates that linear clusters with E.R. less than five behave more like non-linear (2-D) clusters. Only line clusters with E.R. larger than five may be considered to have sufficiently larger length than width to be characterized as linear (or 1-D)

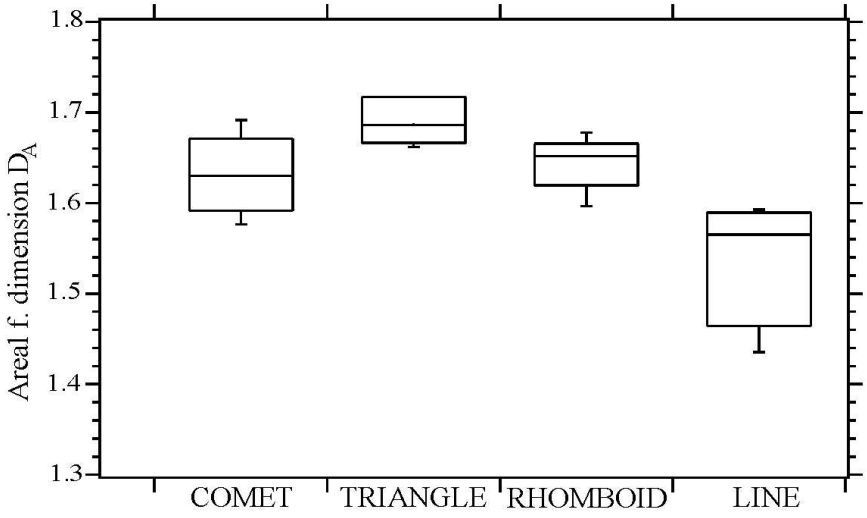


**Fig. 6.** Distribution of $D_A$ per cluster shape considering only one particle wide line clusters. The bottom, middle and top box lines are the 25th, 50th and 75th percentiles, respectively. Bottom and top whiskers are the 5th and 95th, respectively

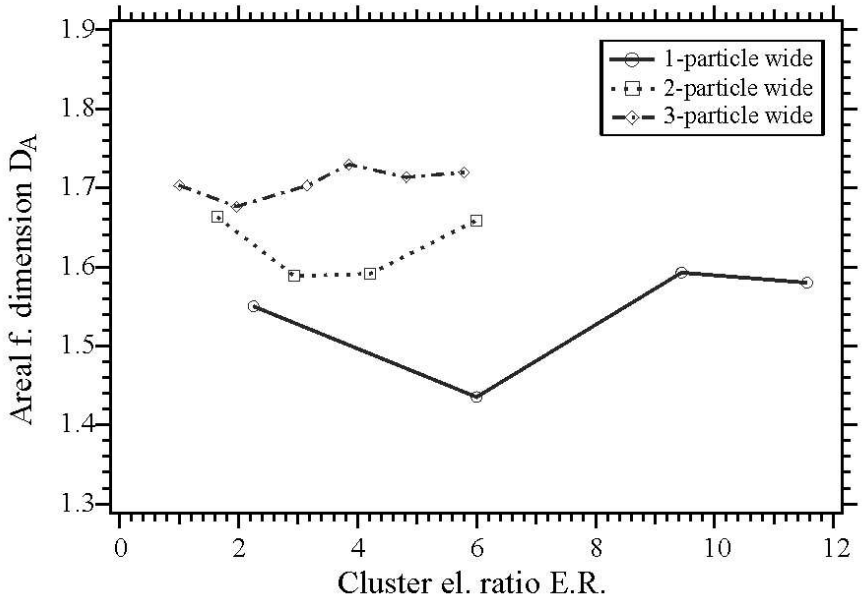


**Fig. 7.** Variation of $D_A$ for linear clusters with cluster E.R.

clusters. This finding also implies that cluster E.R. values should be reported along with $D_A$, when $D_A$ is used to characterize cluster shape.

The distributions of the ordinate intercept terms $b_A$ for each characteristic shape are given in Fig. 8. Rhomboid clusters have a very narrow distribution of $b_A$ values, which are also the lowest among the 2-D cluster shapes. Triangle clusters have the highest values of $b_A$. Comet clusters are the 2-D cluster shape with largest variability in $b_A$ values. The $b_A$ median value is between $b_A$ values of rhomboid and triangle shapes, while the distribution shows a tail which overlaps with the $b_A$ values of triangle clusters. The line clusters have the lowest values of $b_A$ and the greatest variability of $b_A$ values. Therefore Fig. 8 shows that $b_A$ values are dictated by cluster shape. It could be argued that $b_A$ captures a scale-independent aspect of the roughness length magnitude of each cluster shape. A similar finding was reported by Klinkenberg (1992), when investigating landscape roughness. The triangle shape has the greatest irregularity and hence the largest values of $b_A$ among the 2-D shapes. The most "aerodynamic" 2-D shape is the rhomboidal, which has the lowest $b_A$ values of the 2-D shapes. The comet shape is in-between the triangular and the rhomboid shapes and thus has $b_A$ values between the values of the triangle and rhomboid shapes.

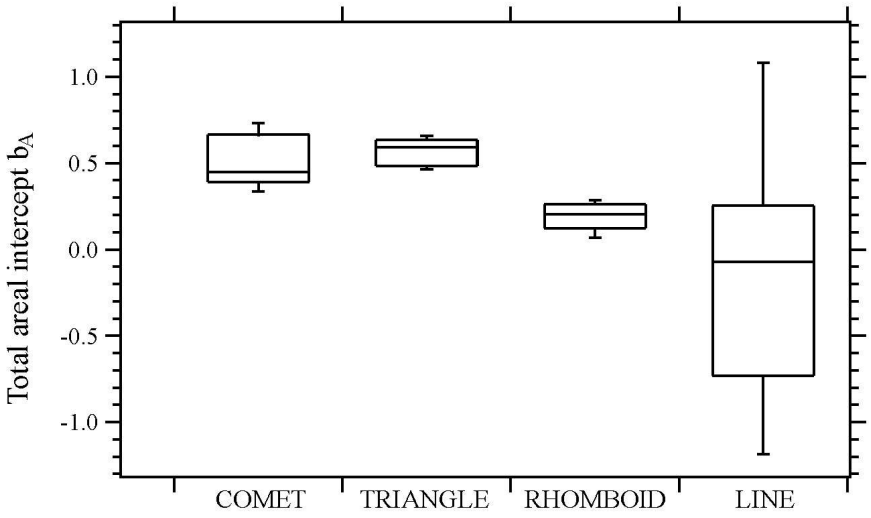


**Fig. 8.** Distribution of $b_A$ per cluster shape. The bottom, middle and top box lines are the 25th, 50th and 75th percentiles, respectively. Bottom and top whiskers are the 5th and 95th percentiles, respectively

Line clusters have $b_A$ values which span from values comparable to ones of non-linear clusters to much lower values. A plot of $b_A$ with the E.R. of linear clusters (Fig. 9) shows that $b_A$ is correlated with the E.R in the case of line clusters. When

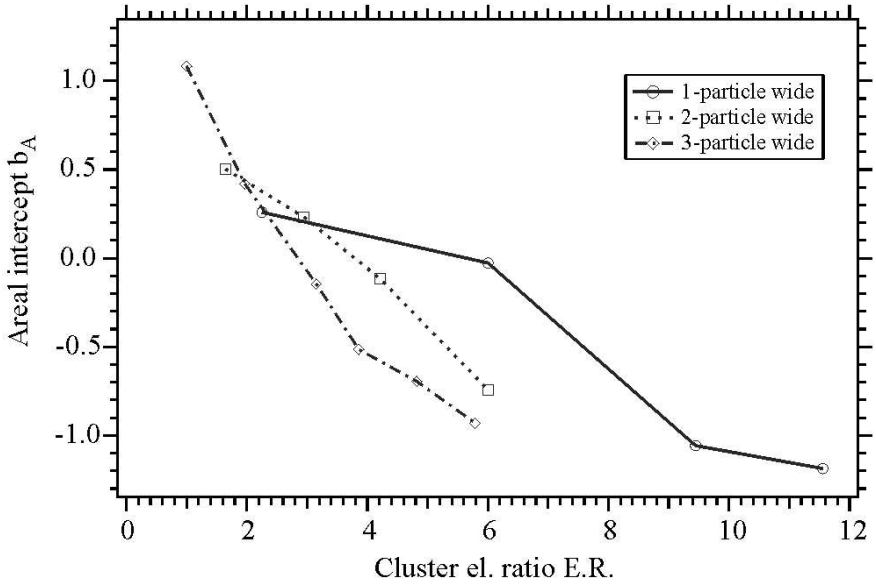


**Fig. 9.** Variation of $b_A$ with cluster elongation ratio, E.R., for linear clusters only

E.R. is roughly equal to one, cluster shape resembles the square shape, which is less "aerodynamic" than the triangle shape. Therefore, line clusters with E.R. close to one present greater $b_A$ values than 2-D clusters. As line clusters become more elongated, their roughness decreases until E.R. becomes greater than roughly five. Beyond the threshold value of E.R. equal to five, $D_A$ shows very small variation.

In order to employ the synthetic cluster results for the classification of the laboratory clusters into the characteristic shape categories, all three parameters, i.e. $D_A$, $b_A$ and E.R. of the laboratory clusters should be considered. Therefore, the $D_A$ and $b_A$ values of each laboratory cluster are compared with the benchmark $D_A$ and $b_A$ values, respectively (Figs. 6 and 8), of the synthetic clusters having similar E.R. A laboratory cluster is classified to a characteristic shape category only if both $D_A$ and $b_A$ classify the laboratory cluster to the same shape category. Otherwise, the cluster is considered as unidentified. The outcome of the cluster shape taxonomy with the proposed areal method is presented in Table 1.

The shape characterization of the majority (84%) of the clusters yielded by the areal method was confirmed via visual observation. Consequently, the shape of these clusters is objectively determined. For the remaining 16% of the laboratory clusters, the areal method did not agree with the visual observation with respect to the characterization of cluster shape. A more in-depth examination revealed that 87% of the clusters of this category were visually identified as comet clusters, while the employed areal method classified them either as linear or rhomboid. It is, thus,

**Table 1.** Comparison of the areal method (denoted as "A") and the visual observation (denoted as "V") for the laboratory clusters

| Category | Visual ID possible | | | No visual ID possible | | |
|---|---|---|---|---|---|---|
| | V, A agree | V, A disagree | Sum | ID with A but not V | NO ID with V or A | Sum |
| Cluster No. | 78 | 15 | 93 | 13 | 17 | 30 |
| Cluster % (of category) | 83.87 | 16.13 | 100 | 43.33 | 56.67 | 100 |
| Cluster % (of total) | 63.41 | 12.20 | 75.61 | 10.57 | 13.82 | 24.39 |

suggested that the comet shape is a transitional stage between linear and non-linear shapes during cluster evolution (Fig. 6).

Approximately 25% of the 123 laboratory clusters could not be identified visually. The areal method classified roughly half of these laboratory clusters as linear, whereas the shape of the remaining half could not be identified. This result implies that the clusters of this category do not exhibit the characteristics of each characteristic cluster shape at degree that would allow cluster shape classification either with the areal method or visually. This could be an indication that the laboratory clusters of this category are in a transitional stage of their shape evolutionary cycle.

## 4. Conclusions

The present study introduced a method for the characterization of cluster shape in quantitative terms based on concepts of fractal geometry. The cell counting technique was utilized for the estimation of the cluster areal fractal dimension, $D_A$, of fabricated clusters with well-defined shapes and laboratory-generated clusters.

The main contribution of this study is that the proposed method utilizing cluster $D_A$ successfully led to the characterization of laboratory clusters, mimicking naturally occurring clusters. At the same time, the findings of this study highlighted the importance of the cluster E.R., which has not been considered before for cluster characterization.

Characterization of cluster shape is of key importance, when modeling flows over microroughness elements such as clusters. Knowing the characteristic $D_A$, adjustments to the grid size distribution of numerical models can be performed. Grid size should be adjusted to represent the geometric attributes of clusters. Quantitative shape information is also important for the selection of the appropriate model for each cluster type. For example, a 2-D cluster shape would require a 3-D model for the resolution of the turbulent flow field around a cluster (Strom et al 2007), whereas in the case of an 1-D cluster a 2-D model would still give meaningful results. Furthermore, knowledge of cluster shape could improve the interpretation of the results from such models, since the shape of roughness elements significantly affects their surrounding turbulence patterns (Schlichting 1936).

With that line of thinking, the impact of this research will be broader, with implications that extend beyond cluster shape characterization. Hence, the cell counting method as proposed here could be important for pattern recognition studies of stream reaches with other ubiquitous bedforms (e.g. bifurcate bars) and for performing dynamic surveys of gravel bed rivers throughout of a hydrologic cycle. Further research will explore the utility of CCM in natural gravel bed streams. Images of the bed will be reconstructed by the use of a LIDAR system.

## 5. Aknowledgements

The authors would like to acknowledge the support provided by the NSF Hydroscience division under NSF grant EAR-0208358.

## References

Andrle R. (1996) Complexity and scale in geomorphology: Statistical self-similarity vs. characteristic scales, *Mathematical Geology*, **28** (3), 275–293.

Bluck B. J. (1987) *Bed forms and clast size changes in gravel bed rivers*, In: *River Channel Environment and Process* (Eds. K. S. Richards), Institute of British Geographers Special Publication, No. 17, 159–178, Blackwell, Oxford.

Brayshaw A. C. (1984) *Characteristics and origin of cluster bedforms in coarse grained alluvial channels*, In: *Sedimentology of Gravels and Conglomerates* (Eds. E. H. Koster and F. J. Steel), *Canadian Society of Petroleum Geologists*, **10**, 77–85.

Buczkowski S., Kiriakos S., Nekka F., Cartiller L. (1998) The modified box-counting method: Analysis of some characteristic parameters, *Pattern Recognition*, **31** (4), 411–418.

Buffin-Bélanger T., Roy A. G. (1998) Effects of a pebble cluster on the turbulent structure of a depth-limited flow in a gravel bed river, *Geomorphology*, **25**, 249–267.

Cheng Q. (1995) The perimeter-area fractal model and its application to Geology, *Mathematical Geology*, **27** (1), 69–82.

de Jong C. 1995 Temporal and spatial interactions between river bed roughness, geometry, bedload transport and flow hydraulics in mountain streams – examples from Squaw Creek, Montana (USA) and Schmiedlaine/Lainbach (Upper Germany), *Berliner Geographische Abhandlungen*, **59**.

Dubuc B., Quiniou J. F., Roques-Carnes C., Tricot C. and Zucker S. W. (1989) Evaluating the fractal dimension of profiles, *Physical Review A*, **39** (3), 1500–1512.

Hassan A. M., Reid I. (1990) The influence of microform bed roughness elements on flow and sediment transport in gravel bed rivers, *Earth Surface Processes and Landforms*, **15**, 739–750.

Karperien A. (1999–2007) FracLac for ImageJ, version 2.5, http://rsb.info.nih.gov/ij/plugins/fraclac/FLHelp/ Introduction.htm.

Kaye B. H. (1986) The description of two-dimensional rugged boundaries in fineparticle science by means of fractal dimensions, *Powder Technology*, **46**, 245–254.

Klinkenberg B. (1992) Fractals and morphometric measures: Is there a relationship?, *Geomorphology*, **5** (1–2), 5–20.

Klinkenberg B. (1994) A review of methods used to determine the fractal dimension of linear features, *Mathematical Geology*, **26** (1), 23–46.

Kozlowski B., Ergenzinger P. (1999) Ring structures – a specific new cluster type in steep mountain torrents, *27th IAHR Congress*, Graz.

Lacey R. W. J., Roy A. G. (2007) A comparative study of the turbulent flow field with and without a pebble cluster in a gravel bed river, *Water Resources Research*, **43**, W05502.

Laronne J. B., Carson M. A. (1976) Interrelationships between bed morphology and bed-material transport for a small, gravel bed channel, *Sedimentology*, **23**, 67–85.

Longley P. A., Batty M. (1989) Fractal measurement and line generalization, *Computers and Geosciences*, **15** (2), 167–183.

Lovejoy S. (1982) Area-perimeter relation for rain and cloud areas, *Science*, **216** (9), 185–187.

Mandelbrot B. (1977) *Fractals, chance, form and dimension*, W. H. Freeman, San Francisco.

Orford J. D., Whalley B. W. (1983) The use of fractal dimension to quantify the morphology of irregular-shaped particles, *Sedimentology*, **30** (5), 655–668.

Papanicolaou A. N. (1999) Stochastic considerations in hydraulics – A call for papers, *Journal of Hydraulic Engineering*, **125** (12), 1229–1230.

Papanicolaou A. N., Diplas P., Dancey C. L. and Balakrishnan M. (2001) Surface roughness effects in near-bed turbulence: implications to sediment entrainment, *Journal of Engineering Mechanics*, **127** (3), 211–218.

Papanicolaou A. N., Strom K., Schuyler A. and Talebbeydokhti N. (2003) The role of sediment specific gravity and availability on cluster evolution, *Earth Surface Processes and Landforms*, **28**, 69–86.

Papanicolaou A. N., Kramer C. (2005) The role of relative submergence on cluster microtopography and bedload predictions in mountain streams, *Proceedings of the International Symposium, IAHR, River, Coastal and Marine Morphodynamics*, IL, October.

Rasband W. S. (1997–2000) ImageJ U. S. National Institutes of Health, Bethesda, Maryland, USA, http://rsb.info.nih.gov/ij/.

Reid I., Frostick L. E., Brayshaw A. C. (1992) Microform roughness elements and the selective entrainment and entrapment of particles in gravel bed rivers. In: *Dynamics of Gravel Bed Rivers* (Eds. Billi P., Hey R., Thorne C. R., Tacconi P.), John Wiley & Sons Ltd., Chichester, 253–275.

Schlichting H. (1936) Experimentelle untersuchungen zum rauhigkeitsproblem, *Ing.-Arch.*, **7**, 1–34.

Strom K., Papanicolaou A. N., Evangelopoulos N. and Odeh M. (2004) Microforms in gravel bed rivers: formation, disintegration and effects on bedload transport, *Journal of Hydraulic Engineering*, **130** (6), 554–567.

Strom K. B. and Papanicolaou A. N. (2007) Morphological characterization of cluster microforms, *Sedimentology*, **55** (1), 137–153.

Strom K. B., Papanicolaou A. N. and Constantinescu G. S. (2007) Flow heterogeneity over a 3D cluster microform: a laboratory and numerical investigation, *Journal of Hydraulic Engineering*, **133**, 273–287.

Teisseyre A. K. (1977) Pebble clusters as a directional structure in fluvial gravels: Modern and ancient examples, *Geologica Sudetica*, **12** (2), 79–89.

Whalley W. B., Orford J. D. (1989) The use of fractals and pseudofractals in the analysis of two-dimensional outlines: Review and further exploration, *Computers and Geosciences*, **15** (2), 185–197.

Whittaker J. G., Jaeggi M. N. R. (1982) Origin of step-pool systems in mountain streams, *Journal of the Hydraulic Division of the American Society of Civil Engineers*, **108** (6), 758–773.

Wittenberg L. (2002) Structural patterns in coarse gravel river beds: typology, survey and assessment of the roles of grain size and river regime, *Geografiska Annaler*, **84A**, 25–37.

Woronow A. (1981) Morphometric consistency with the Hausdorff-Besicovich dimension, *Mathematical Geology*, **13** (3), 201–216.